Phase-Locking of a Second-Harmonic Gyrotron Oscillator Using a Quasi-Optical Circulator to Separate Injection and Output Signals* .

H. Z. Cue, D.J. Hoppe, MEMBER, IEEE, J. Rodgers, R.M. Perez,

J.P. Tate, MEMBER, IEEE, Il.].. Conroy, V. I.. Granatstein, FELLOW, IEEE, A. Bhanji,

P.E. Latham. MEMBER, IEEE, G.S. Nusinovich, SENIOR MEMBER, IEEE,

and M. Naiman

Phase-locking in a 34.5 GHz special complex cavity gyrotron oscillator operating at the second harmonic of the electron cyclotron frequency was studied. Injection of the locking power was made via a quasi-optical circulator connected to the gyrotron output. Locking bandwidth was measured by comparing the phase of the injection signal and output signal using a balanced mixer. Locking was observed with input power level as low as 40 dB below the gyrotron output power. The locking bandwidth is, however, narrower than in gyrotrons operating at the fundamental cyclotron frequency which may be attributed to the longer resonant cavity in the second harmonic gyrotron and the corresponding larger value of external quality factor. The measurements are roughly in agreement with predictions of Adler's phase-locking equation which is given for our system in terms of powers propagating in the output waveguide toward and away from the gyrotron cavity.

H.Z. Guo, J. Rodgers, V.L. Granatstein, P.E. Latham, G.S. Nusinovich, and M. Naiman are with the Institute for Plasma Research, University of Maryland, College Park, MD 20742.

D.J. Hoppe, R.M. Perez, B.L. Conroy, and A. Bhanji are with the Jet Propulsion Laboratory, Pasadena, CA 91109.

J.P. Tate was with the [University of Maryland and is now with Florida A & M University, Tallahassee, FL 32307.

I. INTRODUCTION

Efficient. high power, coherent millimeter wave sources are currently needed for satellite and space communications and for imaging radar to be used in space exploration [1]. A weakly relativistic (electron energy < 100 keV) gyrotron phase-locked oscillator operating at high harmonic of the electron cyclotron frequency (harmonic number s ≥ 2) has been considered as one of the appropriate source choices for these applications for the following reasons:

(1) the transverse dimensions of both the electron brain and the circuit can be much larger than in klystrons or slow-wave microwave tubes because of the ability of gyrotrons to operate in fast wave, higher-order, transverse electric modes, resulting in higher average and peak power rating at a given operating frequency;

(2) the moderate voltage requirement avoids the need for large insulators or electron accelerator sections; and

(3) the required magnetic field can be reduced by tile harmonic factors compared with gy - rotrons operating at fundamental cyclotron frequency, potentially making gyro-devices compatible with modern permanent magnet technology up to operating frequencies of approximately $(s \times 20)$ GHz.

Recently, major advances have been reported in gyrotrons operating at harmonics of the cyclotron frequency. High efficiency and high power have been achieved in free running second harmonic gyrotron oscillators operating in the millimeter-wave band [2-4]. Furthermore, there have been successful demonstrations [5,6] of phase-locked gyrotrons operating at the fundamental cyclotron frequency. However, no phase-locked harmonic gyrotron operation had been reported prior to the present paper.

In this paper we report the operation and measurement of a high power ($\sim$100 kW) second harmonic gyrotron phase-locked by signal injection through the output window using a quasi-optical circulator system [7] to separate the input and output signals. Section II gives a brief description of the second harmonic gyrotron and the arrangement of the phase-locking experiment. Section 111 discusses the pertinent theory of phase-locking taking into account reflection of the injected signal at the entrance to the gyrotron cavity; requirements on the flatness of the voltage pulse applied to the gyrotron are also discussed. In Section

IV the results of the phase-locking experiment are presented and compared with theoretical predictions. Finally, a summary is presented in Section V.

II. DESCRIPTION OF THE GYROTRON AND THE EXPERIMENTAL ARRANGEMENT

A. The Second-Harmonic Gyrotron

A second-harmonic gyrotron which features a novel complex cavity as its beam-wave interaction structure [3] was used for the demonstration of phase-locking. The parameters of this gyrotron, GY-32, are shown in Table 1. Figure 1 is a cross-sectioned drawing of the gyrotron tube along with a typical magnetic field profile. 'l'he special complex cavity consists of five parts as depicted in Fig. 2. Part 1 and part 2 are uniform circular waveguide sections with their inner radii denoted by a and b, respectively. These sections are designed to operate, respectively, in the TE_{02} and TE_{03} modes. In order to couple these two modes into one normal mode of a complex cavity the eigenfrequencies of these two partial modes must be the same. This is accomplished by choosing radii a ant] b to satisfy the condition

$$\frac{\mu_{02}}{a} = \frac{\mu_{03}}{b} = k_c,$$ (1)

where eigennumbers μ_{02} and μ_{03} are roots of the equations $J'(\mu_{02}) = J'(\mu_{03}) = 0$, J_0 is the zero order Bessel function and k_c is the cutoff wavenumber, which is the same for both modes. Then, if the lengths of both sections are also equal that gives closely matched axial wavenumbers for both modes; thus, one can suppose that in a complex cavity these two partial modes will have closely matched eigenfrequencies.

To provide a coupling between these two modes a slotted waveguide with a gradually changing cross section is used (part 3). This part is composed of a main waveguide of radius a and N slotted branch waveguides. The angle subtended by each slot, $2\Theta_0$, varies slowly from O to $2\pi/N$ over the length cd; the depth of each branch waveguide is constant and equal to $(b - a)$. Thus, the gradually changing slotted waveguide efficiently converts a TE_{02} mode to a TE_{03} mode. The three parts described above together with part 4 (cutoff section) and part 5 (diffraction output section) form a resonator. Good mode selectivity results from this kind of complex cavity for the following reasons:

(1) The radial metallic fins at one end of the mode converter function as a mode filter. This is because modes which have a radial component of rf electric field may not be excited in the presence of the radial metallic sheets.

3

(2) The mode converter functions as mode isolator . With the design criterion applied to this case. only one pair of modes (TE_{02} and TE_{03}) will be coupled ant] form a normal mode for the whole system.

Fig. 1. Cross-section of the GY-32 gyrotron tube along with a typical magnetic field profile.

Fig. 2. Special complex cavity with internal mode converter for transforming TE_{02} to TE_{03} (a = 9.65 mm, 6, 14 mm, cavity length $\doteq$ 110 mm).

Table 1. Performance parameters of the GY-32 gyrotron.

Harmonic Number	2
Beam Voltage	40-60 kV
Frequency	34.5 GHz
Beam Current	8-11 A
Peak Output Power	80-230 kW
$\alpha = v_\perp/v_\parallel$	1.5
Efficiency	~35%
Quality Factor, Q	2000
Ohmic Quality Factor, Q_{ohm}	10,000
Mode Purity (TE_{03} mode)	>90%

Due to the superior mode selectivity of the special complex cavity, stable, efficient, harmonic gyrotron operation and high output mode purity result. Both of these are vital for realization of the proposed phase-locking. It would have been more difficult to achieve the required stability of operation in a more usual smooth-wall cavity gyrotron operating at a harmonic of the cyclotron frequency because of mode competition problems. Also, the phase-locking arrangement in the present study employed a quasi-optical circulator for separation of injection signal from the gyrotron output signal, and this circulator has critical demands on gyrotron output mode purity for its effective operation.

Evidence for the stability of gyrotron operation is shown in Fig. 3. Figure 3(a) shows a typical modulator voltage and current pulse; 3(b) is a detected sample of the gyrotron rf output; 3(c) is the gyrotron output frequency spectrum; and 3(d) shows the output mode pattern recorded on a liquid crystal display. All of the above traces were taken prior to

4

injecting the phase-locking signal (i. e., the gyrotron was in a free-running condition). Since gyrotron shot-to-shot stability and instantaneous frequency stability were of great important, gyrotron output power was traded off for increased stability by keeping the beam current and the beam voltage at the lower end of the values shown in Table 1. Lower current reduces beam space charge thereby increasing the coherence of the electron cyclotron phase bunching. Lowering the voltage has the effect of reducing shot-to-shot pulse height fluctuations in the modulator, The gyrotron system operating parameters for the phase-locked experiment are shown in Table 2.

Fig. 3. Stable operation of the GY-32 gyrotron: (a) modulator voltage and current pulses; (b) gyrotron 34.5 GHz output pulse envelope; (c) frequency spectrum of the output signal; and (d) mode pattern of output signal.

Table 2. Operating rameters for the phase-locke yrotron experiment.

Beam Voltage	42-45 kV
Beam Current	8 Amps
Frequency	34.52 GHz
Output Power	80-100 kW
Gun Field	1.15 kG
Cavity Field	6.5 kG
Repetition Rate	43 Hz
Pulse Width	7 μs

B. Experimental Arrangement

A block diagram of the phase-locked system is shown in Fig. 4. A synthesized microwave generator signal amplified by a 100-watt traveling wave tube amplifier (TWTA) provided the injection signal. The signal transmission path included a conventional waveguide isolator providing more than 35 dB of isolation, a directional coupler for sampling the injection signal, and a smooth-wall dual-mode horn providing a gaussian beam for launching into the quasi-optic system.

The quasi-optic circulator is depicted in detail in Fig. 5. The microwave beam was reflected off a fiat plate, focused by an ellipsoidal mirror with focal lengths of 24 and 48

5

inches, and then redirected towards a polarized grid. The grid was fabricated by printing 0.00615 inch copper strips on 0.0123 inch centers on a 0.189 inch thick disk of fused quartz. The beam then passed through the circulator which consists of a 5.75 inch diameter disk of ferrite material, TransTech G-4259, biased with a 1 kGNDFE permanent magnet. The thickness of the disk was chosen to be 0.344 inches, producing a 45 degree Faraday rotation of the microwave beam as it passes through the disk. Fused quartz matching layers of thickness 0.0425 inches were employed on each side of the ferrite disk in order to match to free space. The beam *was* then injected into the high power overmoded waveguide system via an identical ellipsoid and system of fiat mirrors.

The high power overmoded waveguide system consists of a series of circular waveguide mode converters which changed the injected beam from the HE_{11} gaussian mode to the TE_{03} gyrotron operating mode. Due to geometrical/mechanical considerations a mode converter system similar to that considered by Deane [8] was employed. The 1.970 inch diameter output waveguide of the gyrotron was nonlinearly tapered to 1.400 inches, where a four-ripple TE_{03}–TE_{02} mode converter was inserted. A further taper to a 1.00 inch diameter was included and followed by a four-ripple TE_{02}–TE_{01} mode converter. The conversion efficiency of these devices each exceeded 96%. The guide was then bent through an angle of 54.5° over an arc length of 20.0 inches converting the TE_{01} mode to the TM_{11} mode. Since the bend used a sinusoidal curvature distribution rather than a constant radius of curvature, an efficiency of 99.9% was achieved. Finally, a corrugated TM_{11}--$IIE11$ mode converter and horn assembly was used to generate a gaussian beam with the correct waist size to couple into the quasi-optical system *[9]*. An overrnoded directional coupler was also included in the waveguide system, providing test signals for a crystal detector and spectrum analyzer.

The gyrotron output followed the reverse path back to the Faraday rotator where it underwent another 45 degree rotation. Since it was then cross-polarized to the grid, the high power beam was transmitted through the grid and was absorbed by a free-space load. The quasi-optic circulator system including the mode converters was measured to have an insertion loss of 1 dB and an isolation of greater than 25 dB. Waveguide losses reduced the injection signal an additional 1 dB.

Fig. 4. Block diagram of the experiment.

Fig. 5. Quasi-optic. circulator configuration.

A small portion of the gyrotron output power was received by a horn antenna located near the free-space load and was sent to the input port of a balanced mixer. There it was combined with a sample of the injection signal from the waveguide coupler located at the TWTA output. The resulting mixer output voltage which was proportional to the instantaneous phase difference between the output and injection signals, was fed into a digitizing oscilloscope. The digitized data were recorded by a computer and stored for later analysis. Crystal detector waveforms and spectrum analyzer displays were also obtained from a branch circuit in the gyrotron output waveguide.

III. THEORY PREDICTIONS: PHASE-LOCKING EQUATION AND DEMANDS ON GYROTRON POWER SUPPLIES

A. Phase-locking Equations

In order to obtain the phase-locking condition in a direct manner, we start from the gyrotron operation equations presented in reference (1 O]. The reduced gyrotron equations, which describe an annular electron beam interacting with a circular TE_{mn} mode near cutoff, have been described in a number of papers [11- 15]. Here we simply write down the pertinent results. For operation at the sth harmonic, the wave equations arc

$$\left(\frac{d}{d\tau} + \frac{11}{22}\right)F = IFg_r(F) + \frac{A}{2}\cos\psi \tag{2a}$$

$$\frac{d\psi}{d\tau} = \beta - Ig_i(F) - \frac{A}{2F}\sin\psi \tag{2b}$$

where $g = g_r + ig_i$ is the gain functional defined by

$$g(F) = -\frac{1}{F}\int_{-\infty}^{\infty} d\xi f(\xi)\langle p^s e^{i\phi}\rangle.$$

The angle brackets denote an average over initial phase ϕ uniformly distributed between O and 27r. In these equations,

$$p = \frac{p_\perp}{p_{\perp 0}}$$

is the perpendicular momentum normalized to its initial value,

$$\phi = \omega t - s\phi_{gp}$$

7

is the slowly varying gyrophase (ϕ_{gp} is the actual particle gyrophase ,

$$\xi = \frac{2z}{L},$$

is normalized distance where L is the length of the cavity as determined by the Gaussian axial distribution,

$$f(\xi) = e^{-\xi^2} = e^{-(2z/L)^2},$$

and I is the normalized current: i.e.,

$$I = \omega T_p \sqrt{\frac{2}{\pi}} \frac{QI_b}{I_A} \left[\frac{1}{(s-1)!} \left(\frac{sv_{\perp 0}}{2c} \right)^{s-1} \right]^2 \frac{J_{m\pm s}^2(k_\perp r_g)}{J_m^2(\nu_{mn}(\nu_{mn}^2 - m^2))} \tag{3}$$

where $T_p = L/v_{z0}$ is the transit time, v_{z0} and $v_{\perp 0}$ are the axial and perpendicular velocities, respectively, c is the speed of light, Ω_{c0} is the initial relativistic cyclotron frequency, I_b is the beam current, $I_A = 4\pi\epsilon_0 m_0\gamma_0 v_{z0} c^2/q$ is the Alfvén current in mks units with q and m_0 the electron charge and rest mass, respectively, Q is the loaded quality factor of the resonator, $k_\perp$ is the perpendicular wave number ($k_\perp \approx \omega/c$ since we are near cutoff), r_g is the guiding center radius, ν_{mn} is the nth zero of J'_m, the derivative of the mth order Bessel function, and m is the azimuthal mode number. The normalized field amplitude, $Fe^{-i\phi}$, is given in terms of the actual field as

$$Fe^{-i\psi} = \frac{E_0}{B.} \frac{\omega T_p}{2v_{\perp 0}/c} \frac{1}{s!} \frac{sv_{\perp 0}}{(2\ c}{\ )}^{s-1} J_{m\pm s}(k_\perp r_g)$$

where the perpendicular component of the electric field,

$$\mathbf{E}_\perp \equiv \mathrm{Re} \left\{ E_0 k_\perp^{-1} \hat{z} \times \nabla_\perp J_m(k_\perp r) \exp\left[i(m\theta - \omega t) \right] \right\},$$

defines E_0, and ψ is the slowly varying wave phase with respect to the phase of the injected signal. The normalized frequency mismatch, β, is given by

$$\beta = Q \frac{\omega_r - \omega}{\omega_r} \tag{4}$$

where ω_r is the real part of the complex cold cavity resonant frequency. Its imaginary part, which is responsible for losses, is described by the term $1/2$ in the brackets on the left-hand side of Eq. (2a); note that in Eq. (2), τ is the slowly varying time, $\tau = \omega t/Q$. Finally, A is proportional to the field injected into the cavity from an external source.

As discussed in the introduction, this paper is specifically addressed to phase-locking of a harmonic gyrotron with external injection. In this respect, the dependence of the locking bandwidth Δf_L on the input and output power is of practical interest. This quantity can be estimated by setting $d\psi/d\tau = 0$ in Eq. (2 b). Then, we can obtain the following formulae for the maximum and minimum detuning:

$$\beta_{\max} = I g_i + \frac{A}{2F} = Q \frac{\omega_r - \omega_{\min}}{\omega_r} \quad \text{for} \quad \sin \psi = 1 \tag{5}$$

$$\beta_{\min} = I g_i - \frac{A}{2F} = Q \frac{\omega_r - \omega_{\max}}{\omega_r} \quad \text{for} \quad \sin \psi = -1 \tag{6}$$

Now, if we assume that at both $\beta_{\max}$ and $\beta_{\min}$ the imaginary part of the gain function, g_i, and the normalized field amplitudes are the same, then we can obtain the following approximate formulae for the locking bandwidth, $\omega_{\max} - \omega_{\min}$:

$$\frac{A}{F} \cong Q \frac{\omega_{\max} - \omega_{\min}}{\omega_0}; \tag{7}$$

and, for the dependence of phase on the frequency:

$$\psi(\omega) = \arcsin \frac{2(\omega - \omega_0)}{\omega_{\max} - \omega_{\min}}, \tag{8}$$

where the 'hot' resonant frequency of the cavity is ω_0 and $\omega_0 \simeq \omega_r$.

Equation (8) together with Eqs. (5) and (6) indicates that the phase traverses 180 degrees as the signal frequency swings through the full lock bandwidth. This will be important in demonstrating that phase-locking was accomplished during the experiments by injecting an external signal that is swept in frequency.

The locking bandwidth defined by Eq. (7) coincides with Adler's relation [16]. Let us interpret this relation in terms of the input and output power flows propagating in our system in the same waveguide since these power flows can be measured in the experiment. For this purpose let us recall that, according to reference [17], the flow of the power into the cavity, P_{cav}, is related to the flow of the incident wave power, P_{in}, as

$$\frac{P_{cav}}{P_{in}} = \frac{4 Q_e/Q_{ohm}}{(1 + Q_e/Q_{ohm})^2 + A} \tag{9}$$

and in the stationary regime this power, P_{cav}, is equal to the power of ohmic losses in the cavity,

$$P_{cav} = P_{ohm} = \frac{\omega}{Q_{ohm}} \cdot A^2 V. \tag{lo}$$

In Eqs. (9) and (1 O), Q_e and Q_{ohm} are, respectively, the external and ohmic quality factors and are related by $Q_e^{-1} = Q^{-1} - Q_{ohm}^{-1}$. In Eq. (9), $\Delta = 2Q_e(\omega - \omega_0)/\omega_0$ and in Eq. (10) V *is* the resonator volume. At the same time, in the presence of the beam when the microwave power extracted from the beam is much larger than P_{cav}, the output power flow is equal to

$$Pout = \frac{\omega}{Q_e} F^2 V. \tag{11}$$

In Eqs. (10) and (11) we are not concerned with the normalization constant for A and F since they are the same for both, and we are interested only in the ratio of these values. As follows from Eqs. (9)-(11), this ratio is equal to

$$\frac{A}{F} \simeq \sqrt{\frac{P_{in}/P_{out}}{[(1 + Q_e/Q_{ohm})^2 + \Delta^2]}}. \tag{12}$$

In our experiment, the condition $A^2 \ll 1$ is well satisfied so that Eq. (12) reduces to

$$\frac{A}{F} \cong \frac{2}{1 + Q_e/Q_{ohm}} \sqrt{P_{in}/P_{out}}. \tag{13}$$

Substituting the field amplitude ratio given by Eq. (13) into Eq. (7) gives the following equation for the phase-locking bandwidth

$$\frac{\omega_{max} - \omega_{min}}{\omega_0} \cong \frac{2}{Q(1 + Q_e/Q_{ohm})} \sqrt{P_{in}/P_{out}}. \tag{14}$$

For the case of a critically coupled cavity (i.e., $Q_e = Q_{ohm}$) with no power reflection at the cavity entrance, Eq. (14) becomes

$$\frac{\omega_{max} - \omega_{min}}{\omega_0} \sim \frac{1}{Q} \sqrt{P_{in}/P_{out}}. \tag{15}$$

Equation (15) is another common form of Adler's equation; however, it is not applicable to the present case since the gyrotron cavity is overcoupled $(Q_e < Q_{ohm})$. Then, one must use the more general form in Eq. (14), which can be rewritten

$$\frac{\omega_{max} - \omega_{min}}{\omega_0} \cong \frac{2}{Q_e} \sqrt{P_{in}/P_{out}}. \tag{16}$$

10

Equation (16) may be regarded as a generalization of Adler's equation which allows for power reflection at the entrance to the cavity.

B. Expected Pulse Waveform

In the experiment, the lock range can be determined by sweeping the synthesizer frequency across the normal operating frequency of the gyrotron and viewing the phase difference between the gyrotron output and the injected signal over a single pulse as well as on a pulse-to-pulse basis.

The average value of the phase difference between the reference and test signals over a given pulse is estimated by computing the average of a set of samples taken from the center portion of the difference pulse. When the difference frequency is large, many cycles appear across the pulse and the average voltage is zero. When the two input frequencies to the mixer are close enough so that no significant portion of a cycle appears across the pulse, a finite average mixer voltage is found for that particular pulse. If the injection signal is so close to the gyrotron frequency that the difference is not resolvable over the pulse length, but the gyrotron is not phase-locked with the injection signal we would expect uncorrelated phase (average pulse voltage) from pulse to pulse. When the gyrotron is injection locked we expect the phase to ramp through a 180 degree range as the locking bandwidth is traversed (see the next section). An example of average voltage results over three regions (high frequency beat note, uncorrelated phase difference, and phase-locked) are shown in Fig. 6. In addition to the average phase of the pulse, the standard deviation of the mixer voltage (pulse phase) is also included on the plot. This statistic is also an aid in determining the lock range. When many cycles appear across the pulse the standard deviation is high; it is low under locked conditions regardless of the phase of the pulse.

Fig. 6. Expected phase vs. injected frequency over three regions: (1) high frequency beat note, (2) uncorrelated phase difference, and (3) phase-locked for the specific case where the 180° range of phase difference is from 0° to 180°.

C. Demands on Gyrotron Beam Voltage

In real systems, there are always voltage fluctuations which change the hot cavity resonant frequency, co.. For phase-locking to occur, frequency changes caused by the voltage

fluctuations, which we denote $\Delta\omega_v$, must be smaller han the locking bandwidth, $\Delta\omega_L$. Combining this condition with Eq. (16) yields

$$\Delta\omega_{v} < \frac{2\omega_0}{Q_e}\sqrt{\frac{P_{in}}{P_{out}}}. \tag{18a}$$

Writing $\Delta\omega_v = \Delta V_b d\omega_0/dV_b$, where ΔV_b is the voltage fluctuation, we have

$$\frac{\Delta V_b}{V_b} < \sqrt{\frac{P_{in}}{P_{out}}} \frac{2\omega_0}{V_b Q_e (d\omega_0/dV_b)} \tag{18b}$$

In this equation, $\Delta V_b/V_b$ is to be interpreted as the allowed relative voltage fluctuation in the modulator. Thus, if $V_b d\omega_0/dV_b$ is too large, it will be impossible to construct a voltage modulator with small enough fluctuations to satisfy Eq. (18). We reproduce here the calculated results which appeared in reference [10] and which are shown in Fig. 7. Allowed maximum values of $\Delta V_b/V_b$ are plotted versus voltage for various values of the detuning parameter δ which is given by

$$\delta = \frac{\omega T_p}{2} \left(1 - \frac{s\Omega_{c0}}{\omega} \right) \tag{19}$$

where Ω_{c0} is the initial relativistic cyclotron frequency.

In these figures, the assumption was made that $P_{in}/P_{out} = 10^{-3}$ and that $Q_e = 1000$. The value of Q_e and the range of V_b do not match those in the present experiment, but the trend of the predictions are believed to be relevant. Gyrotron efficiency is also included on the plots. In the region where the efficiency is below approximately 20%, the requirement on the modulator voltage fluctuations are quite stringent: on the order of 0.1%. On the other hand, for gyrotron efficiency $\gtrsim 30\%$, the allowed voltage fluctuations are typically on the order of 1 %.

IV. EXPERIMENTAL RESULTS

A. Measurement of Locking Bandwidth

In all, sixteen separate experiments were performed. Two were control experiments with the injection horn blocked, eight were performed at full injection power (60 Watts), and two were performed at each of three reduced power levels, (30, 15, and 6 Watts). For each experiment 250 pulses were captured near the center of the lock range for later analysis. The synthesizer was swept across a 10 MHz range in 60 seconds, and the pulse repetition frequency was 43 Hz, corresponding to a frequency step of 3.876 kHz per pulse. The pulse

12

waveforms were sampled at a rate of 10 samples per microsecond, and the effective pulse width was 4 microseconds. In some instances the 250 pulses did not straddle the complete locking bandwidth and no useful results were obtained from those experiments.

Figure 8 plots the average mixer voltage (proportional to the sine of the phase), using a solid line over each of the 250 pulses for a control experiment where the injection horn was blocked. As expected, near the beginning and near the end of the data the difference frequency is large enough to produce at least one complete cycle across the pulse and zero average voltage is obtained. Between pulse 50 and 100 the difference frequency is small, and only the random pulse-to-pulse phase jitter of tile gyrotron is seen. No pulse-to-pulse correlation is observed and the average voltage fluctuates wildly across the entire allowable mixer range of 0.35 to —0.25 volts. Note the fact that these two voltage extremes are not symmetric, indicating a non-ideal mixer with some finite offset voltage. This plot is exactly what one would expect for the control experiment with no injection power. The standard deviation of the voltage samples on each pulse is plotted as a dashed curve in Fig. 8.

Fig. 8. Mean and standard deviation of samples (no locking).

Figure 9 plots the same information for the case when the termination is removed and *60* Watts are injected into the gyrotron. Now a constant phase progression covering the full mixer range (180 degrees) is seen from pulse number 50 to 164. This 114 pulse interval then represents the locking bandwidth, which in this case corresponds to 44o kHz. It can also be observed that at the high end of the lock range, near pulse number 160, there is a region where intermittent locking occurs. This can be attributed to the limited pulse-to-pulse stability as well as the long term drift of the gyrotron frequency. Including the intermittent region, locking occurs over a bandwidth of 510 kHz.

Examination of the individual pulses in the locking range shows that the behavior predicted in Fig. 6 is observed. Figure 10 plots the mixer voltage for four representative pulses captured during the experiment discussed above. As can be seen from Fig. 9, pulse number 3 is unlocked and more than a complete cycle of beat note is visible across the pulse. Pulses numbered 75, 120, and 140 represent locked pulses. They are relatively flat, with an average voltage that is proportional to the phase difference between the injection and output signals. This voltage varies from a maximum (pulse 75) through zero (near pulse 120) to a minimum

(pulse 140) as the lock range is traversed.

Fig. 9. Mean and standard deviation of samples (locked 114 pulses - 440 kHz).

In all, twelve of the experiments produced useful results. These data are tabulated below
in Table 3 along with theoretical predictions from Eq. (16) with gyrotron output power P_{out}
$= 100$ kW, and the gyrotron operating frequency $f_0 = 34.5$ GHz, and taking $Q_e = 2500$.
There is rough agreement between the experimental values of locking bandwidth and the
theoretical predictions. At the highest values of the injection power, the measured band-
width is somewhat smaller than the theoretical value; this may be due to the ripple in the
gyrotron modulator voltage. We also note that as injection power, P_i, is reduced the locking
bandwidth appears to shrink less rapidly than $\sqrt{P_i}$; however, further study is required before
a definitive statement can be made.

Table 3. Results of phase-locking measurement.

P_{in} (Watts)	Avg. # Pulses Locked	Bandwidth (kHz)	Theoretical Bandwidth (kHz) using Eq. (17)	Gain (dB)
0	0	0	0	0
6	68	230--310	220	42
15	79	310--330	348	38
30	90	340--390	490	35
60	106	440--510	693	32

B. Effect of Beam Voltage on Gyrotron Operation

The phase-locking experiment was performed with a gyrotron operating efficiency of 30% and with a beam voltage ripple of 0.3%. These conditions are compatible with theoretical estimates for the realization of phase-locking as suggested by Fig. 7. In fact. the pulse width of the beam voltage was 7 microseconds, but the duration of the microwave signal over which phase-locking could be realized was 4 microseconds. 'l'his 4 microsecond interval corresponds to the flat portion of the beam voltage where $\Delta V_b/V_b < 0.3\%$.

V. DISCUSSION OF RESULTS

The present experiment demonstrated phase-locking of a second-harmonic, 100 kW, millimeter-wave gyrotron oscillator. Locking bandwidth was measured by means of an instantaneously recording and computer processing system. The results demonstrate for the first time phase-locking of a harmonic gyrotron oscillator (s > 1); the phase-locking was accomplished by separating the paths of the injection signal and the output signal in a low 10ss, high power compatible, quasi-optical calculator. 'l'he insights gained during this study may be summarized as follows:

(a) A second-harmonic gyrotron oscillator incorporating a special complex cavity can operate with sufficient stability and efficiency that it can be phase-locked by injecting an external signal as small as 42 dB below the gyrotron output power.

(b) A quasi-optical circulator can be of practical value in phase-locking high power millimeter-wave oscillators with signal injection through the output window.

(c) The requirement for gyrotron power supply stability to achieve phase-locking is quite demanding but can be realized if gyrotron efficiency is high (i.e., $\Delta V_b/V_b \lesssim 0.3\%$ is required if efficiency is $\gtrsim 3070$).

(d) Measured values of locking bandwidth roughly agree with the predictions of a generalized Adler's equation. The measured values of locking bandwidth for a given value of the ratio, P_{in}/P_{out}, were much smaller in the present study than in a previous study of a gyrotron operating at the fundamental of the electron cyclotron frequency [5]; the difference is expected, and is attributable to the longer cavity length and correspondingly larger value of Q_e in the gyrotron of the present study.

15

References

1. R.K. Parker and R.H. Abrams, "Radio-frequent.y vacuum electronics: Resurgent technology for tomorrow ," SPIE vol. 791, *Millimeter Wave Technology IV and Radio Frequency Power Sources,* pp. 2-12, 1987.

2. H. Guo, 1>. S. Wu, G. Liu, Y.V. Miao, S.Z. Qian, and W.Z. Qin, "Special complex open-cavity and low- magnetic-field big]]-power gyrotron," *IEEE Trans. Plasma Sci.,* vol. 18, pp. *326-333, 1990.*

3. V.E. Zapevalov, S.A. Malygin, V.G. Pavelyev, and Sh. E. Tsimring, "Gyrotrons based on coupled cavities with mode conversion, " *Sov. J. Radiophys.,* vol. *27,* pp. 1194-1199, 1984.

4. S.S. Spira-Hakaarainen, K. Kreischer, and R. Temkin, "Submillimeter-wave harmonic gyrotron experiment," *IEEE Trans. Plasma Sci.,* vol. 18, pp. 334-342, 1990.

5. M.E. Read, R. Seeley, W. Manheimer, "Observations of phase locking in a single-cavity gyrotron oscillator," *IEEE Trans. Plasma Sci.,* vol. 13, pp. 398-403, 1985.

6. A.H. McCurdy, C.M. Armstrong, W.M. Bollen, R.K. Parker, and V.L. Granatstein, "Improved oscillator phase locking by use of a modulated electron beam in a gyrotron," *Phys. Rev. Lett, vol. 57,* pp. 2379-2382, 1986.

7. G.F. Dionne, J.A. Weiss, G.A. Allen, and W.D. Fitzgerald, "Quasi-optical ferrite rotator for millimeter waves," Proc. IEEE; MTT-S Int. Microwave Symp. 1, New York, May 17-25, pp. 127-130, 1988.

8. D.L. Deane, "Mode converters for generating the HE_{11} (Gaussian-like) mode from TE_{01} in a circular waveguide," *Int. J. Electronics,* vol. 53, pp. 573-585, 1982.

9. D.J. Hoppe, "A 35 GHz, 200 kW CW TM_{11}-HE_{11} mode converter for gyrotron applications," Proc. IEEE Antennas and Propagation International Symposium, Seattle, June 19-24, pp. 1944-1947, 1994.

10. P.E. Latham, V. I. Granatstein, and Y. Carmel, "Phase locking and bandwidth in a gyrotron oscillator, " *Int. J. Infrared and Millimeter Waves*, vol. 14, no. 6, pp. 1217-1227, 1993.

11. V.A. Flyagin, A.V. Gaponov, M.I. Pete] in, and V.K. Yulpatov, "The gyrotron," *IEEE Trans. Microwave Theory Tech.,* vol. MTT-25, pp. 514-521, 1977.

12. A.W. Fliflet, M.E. Read, K.R. Chu, and R. Seeley, "A self-consistent field theory for gyrotron oscillators: application to a low Q gyromonotron," *Int. J. Electron.*, vol. 53, pp. 505-522, 1982.

13. T.M. Tran, B.G. Danly, K.E. Kreischer, J.B. Schutkeker, and R. J. Temkin, "Optimiza-ion of gyroklystron efficiency," *Phys. Fluids.* vol. *29,* pp. 1 274-1281, 1986.

14. B. Levush and T.M. Antonsen, Jr., "Mode competition and control in high-power gyrotron oscillators," *IEEE Trans. Plasma Sci., vol. 1'S-]/3, pp. 260-272,* 1990.

15. V.S. Ergakov and M.A. Moiseev, "Theory of synchronization of oscillations in a cy-clotron resonance maser monotron by an external signal," *Radiophys. and Quantum Electron., vol.* 18, pp. 89-97, 1975.

16. R. Adler, "A study of phase-locking phenomena in oscillators," Proc. IRE, vol. 34, pp. 351-357, 1946.

17. J.C. Slater, *Microwave Electronics* (D. Van Nostrand Co., Princeton, 1950), p. 95.

FIG. 1

Figure 1. Cross-Section of GY-32 Gyrotron
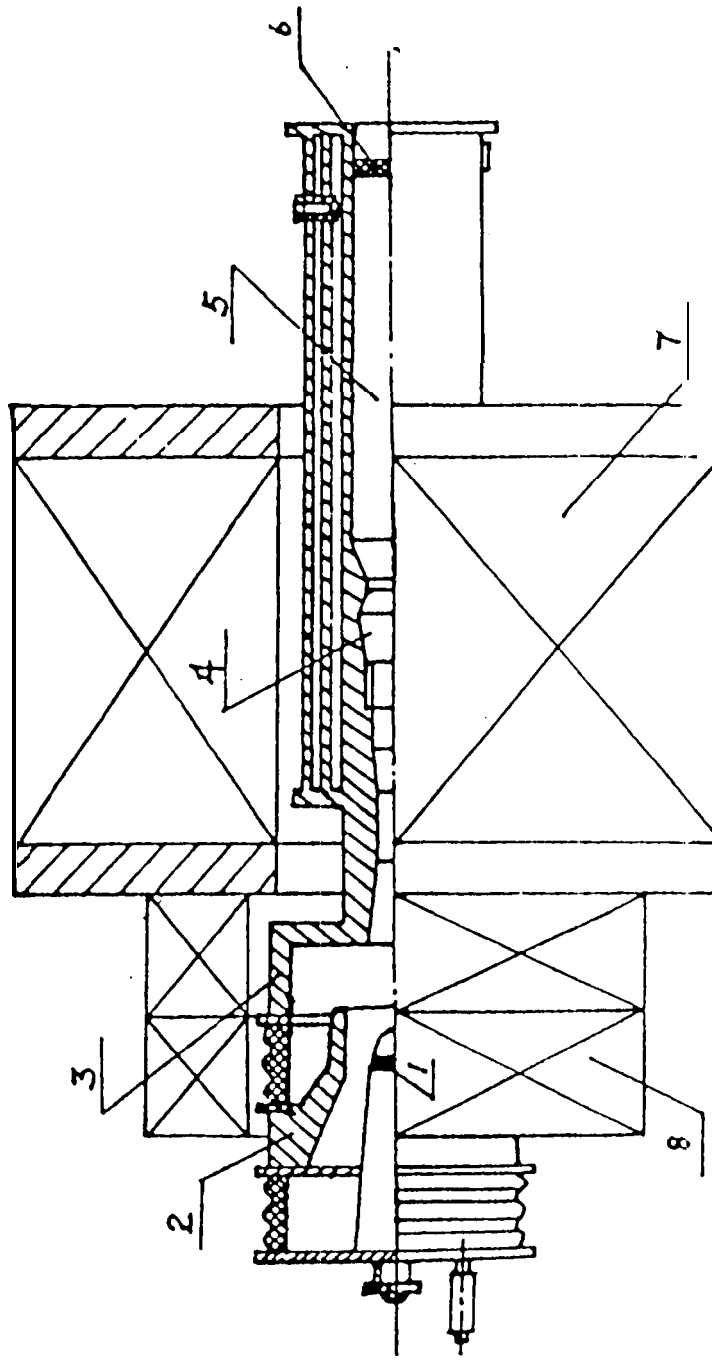
Cathode; 2. Control Anode; 3.Second Anode; 4. Complex Cavity; 5. Beam Collector;
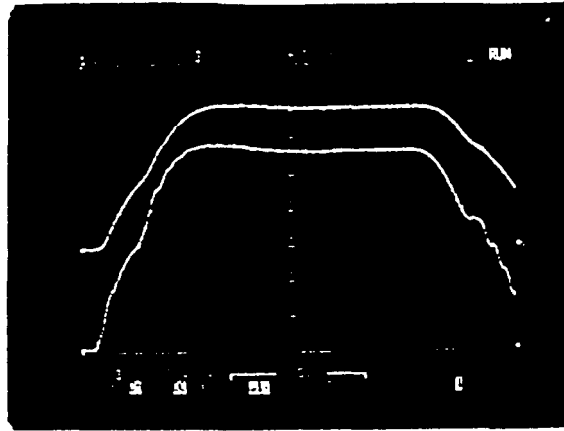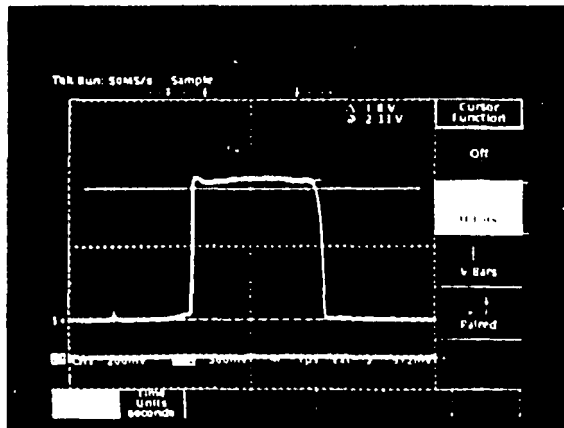6. Output Window; 7. Main Magnetic Feild Coils; 8. Gun Coils
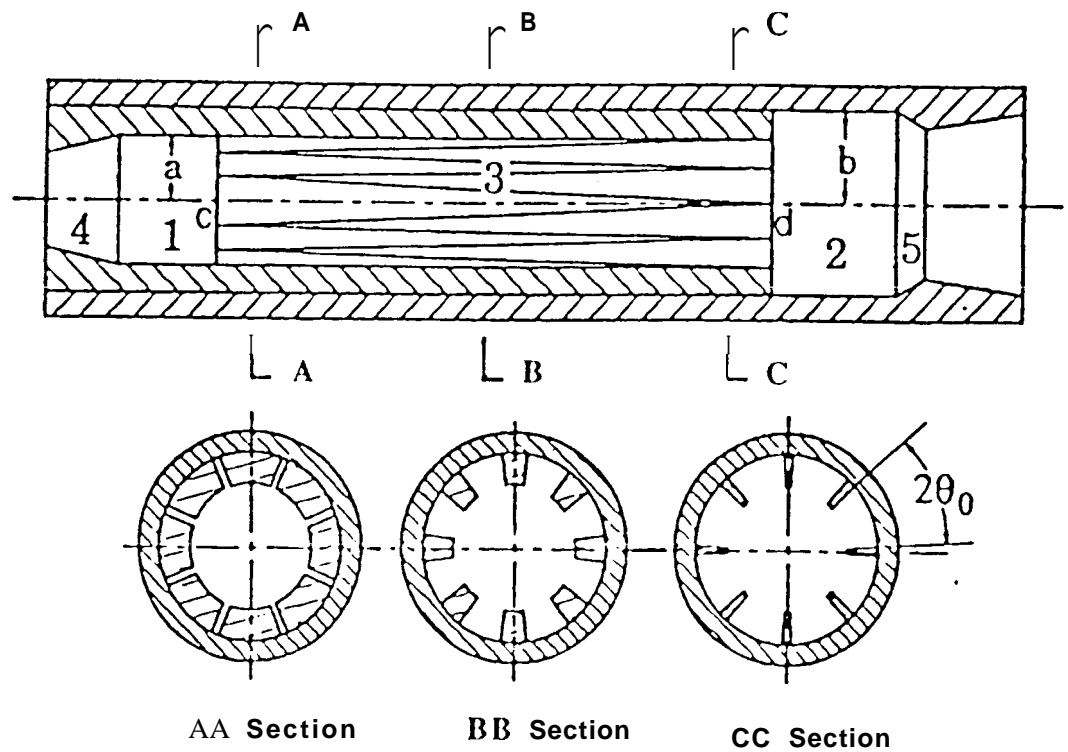
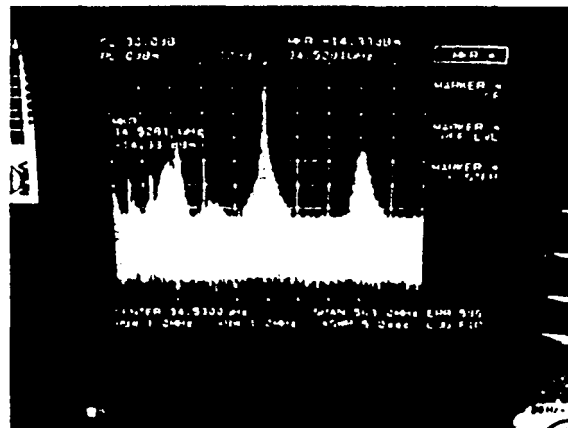Figure 2 Special Complex Cavity With Mode Converter Transforming TE_{02} to TE_{03} Mode
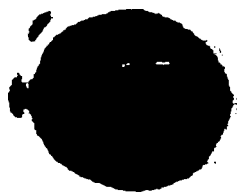
Figure 3

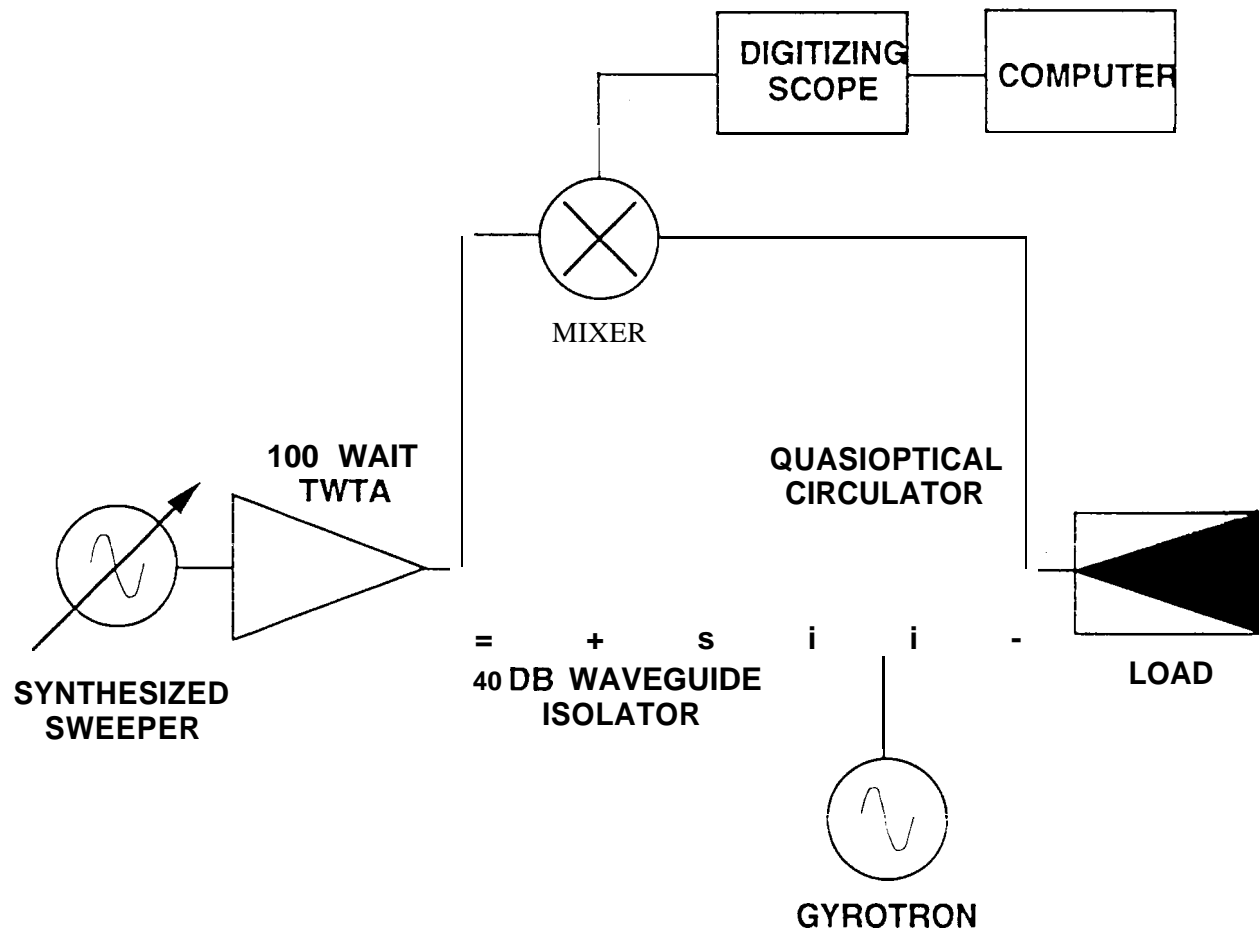(a) Top trace is the modulator voltage 10 kV/div. **Bottom trace** is the beam current. 2 .\/div. Horizontal time axis. 1 μsec/div.
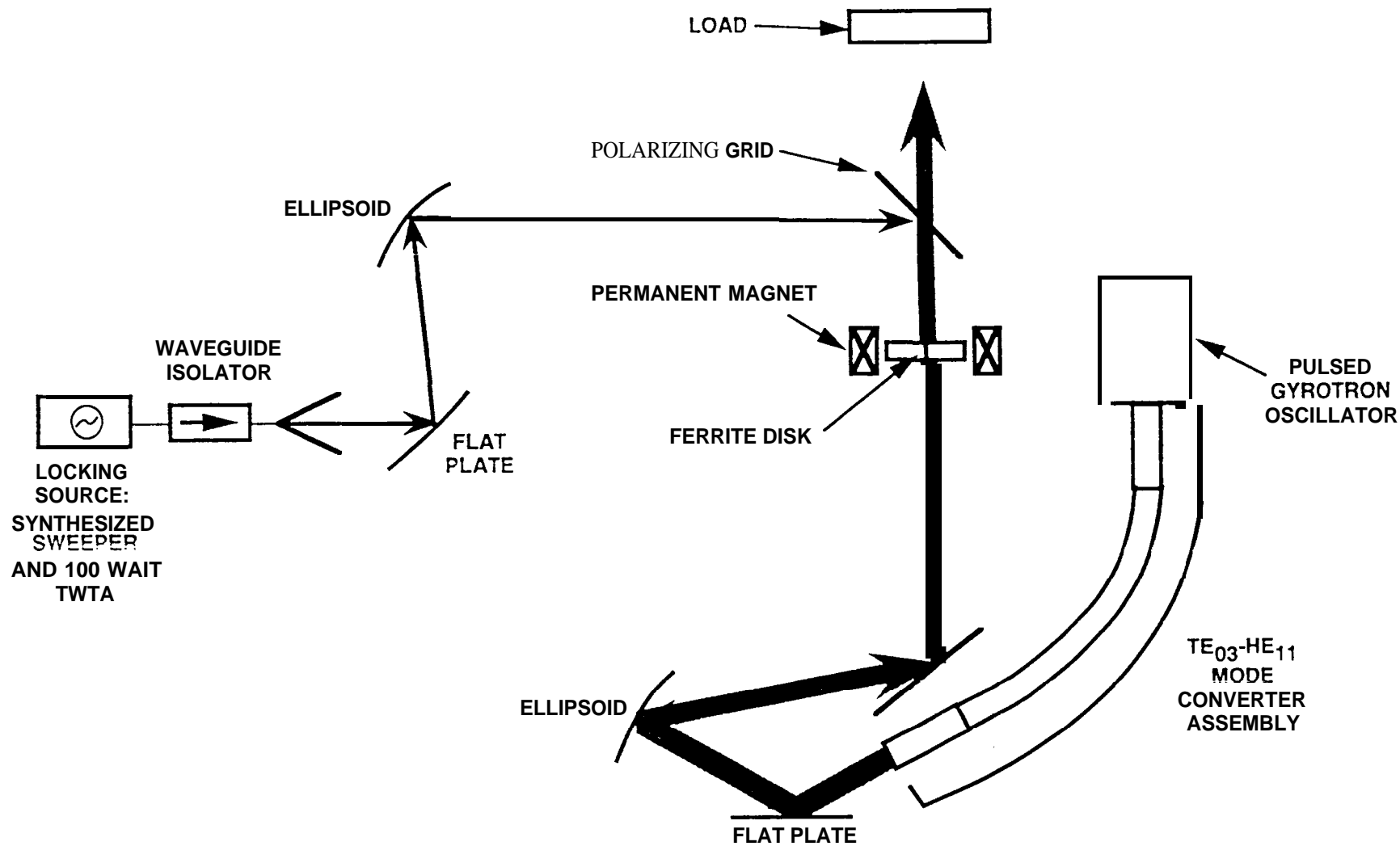

(b) Detected gyrotron output pulse.

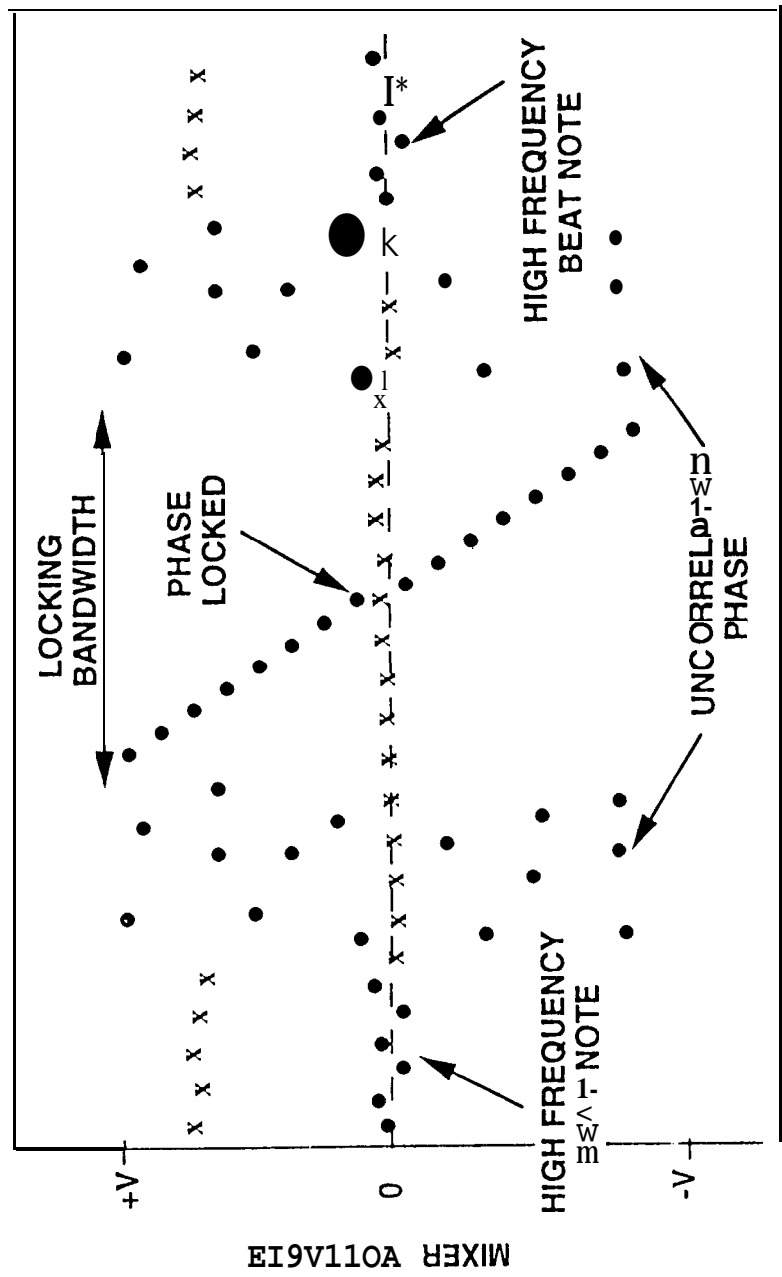(c) Spectrum analyzer display of gyrotron output.

(d) Mode pattern produced in liquid crystal by gyrotron output. TE_{03} mode.

DIGITIZING SCOPE

COMPUTER

MIXER

100 WAIT TWTA

QUASIOPTICAL CIRCULATOR

SYNTHESIZED SWEEPER

= + s i i -

40 DB WAVEGUIDE ISOLATOR

LOAD

GYROTRON

FIG. 4

LOAD

POLARIZING **GRID**

ELLIPSOID

PERMANENT MAGNET

**WAVEGUIDE
ISOLATOR**

FERRITE DISK

**PULSED
GYROTRON
OSCILLATOR**

**LOCKING
SOURCE:**

**SYNTHESIZED
SWEEPER**

**AND 100 WAIT
TWTA**

**FLAT
PLATE**

ELLIPSOID

**TE$_{03}$-HE$_{11}$
MODE
CONVERTER
ASSEMBLY**

FLAT PLATE

● MIXER VOLTAGE (PHASE DIFFERENCE) (AVERAGED OVER PULSE)

x STANDARD DEVIATION OF THE MIXER VOLTAGE OVER PULSE

LOCKING
BANDWIDTH

PHASE
LOCKED

UNCORRELATED
PHASE

I*

k

x_1

HIGH FREQUENCY
BEAT NOTE

$-\omega_n$

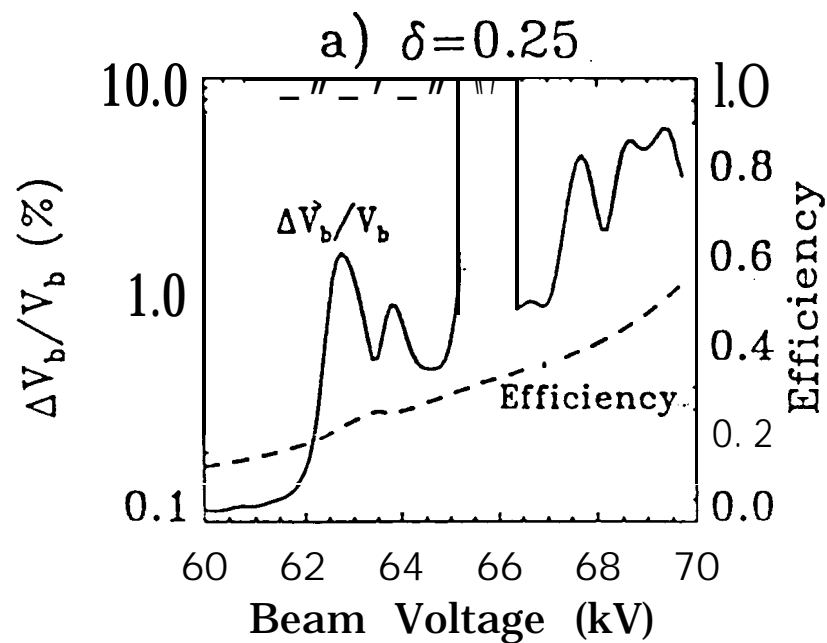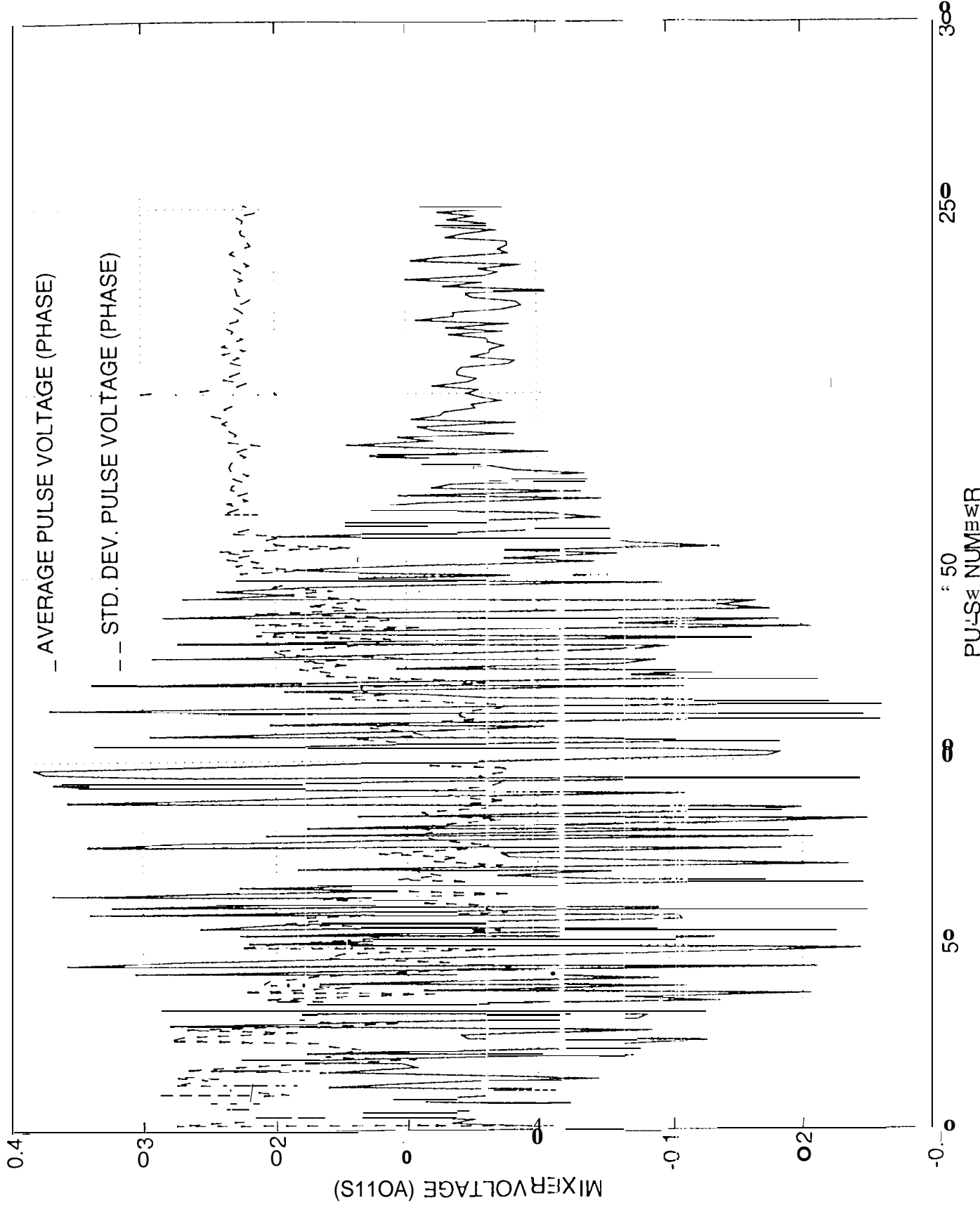$-\omega_m$

HIGH FREQUENCY
NOTE

+V

0

-V

MIXER VOLTAGE

INJECTED FREQUENCY
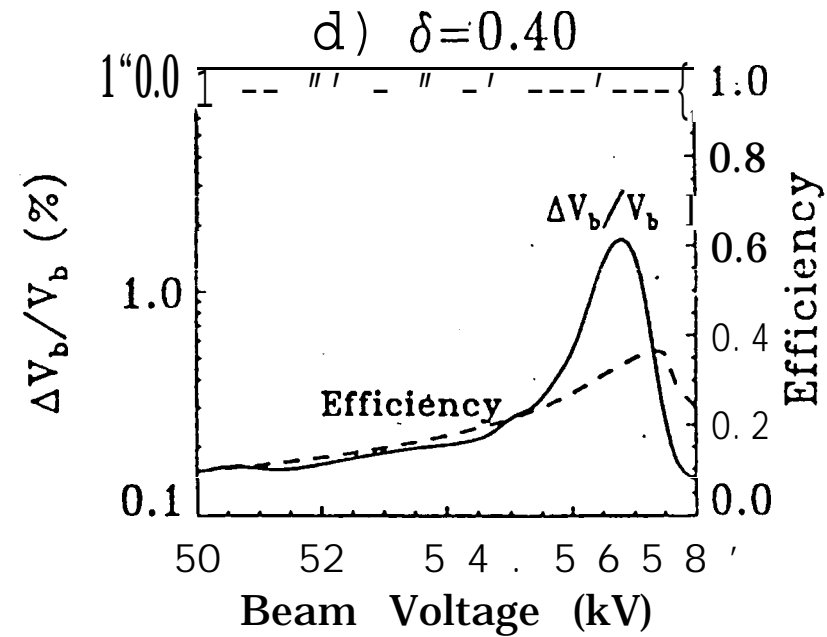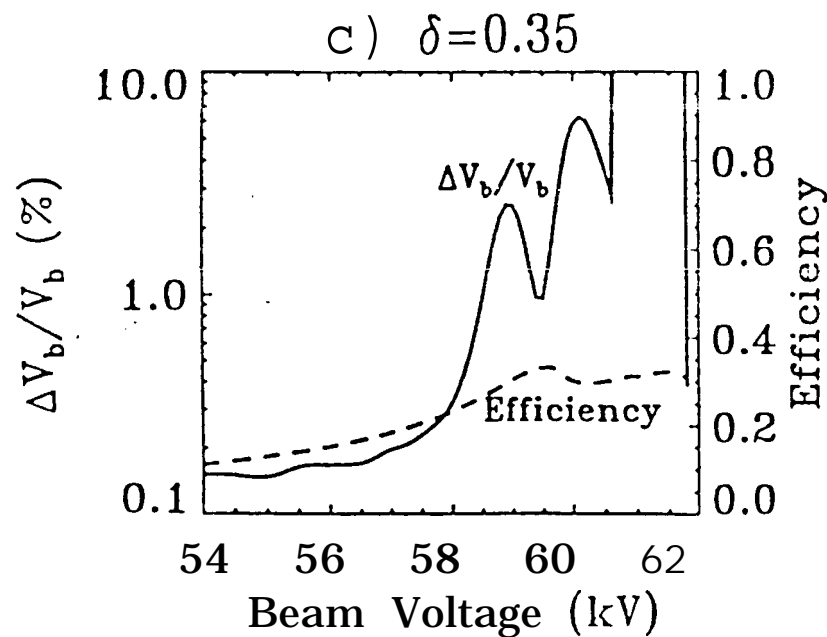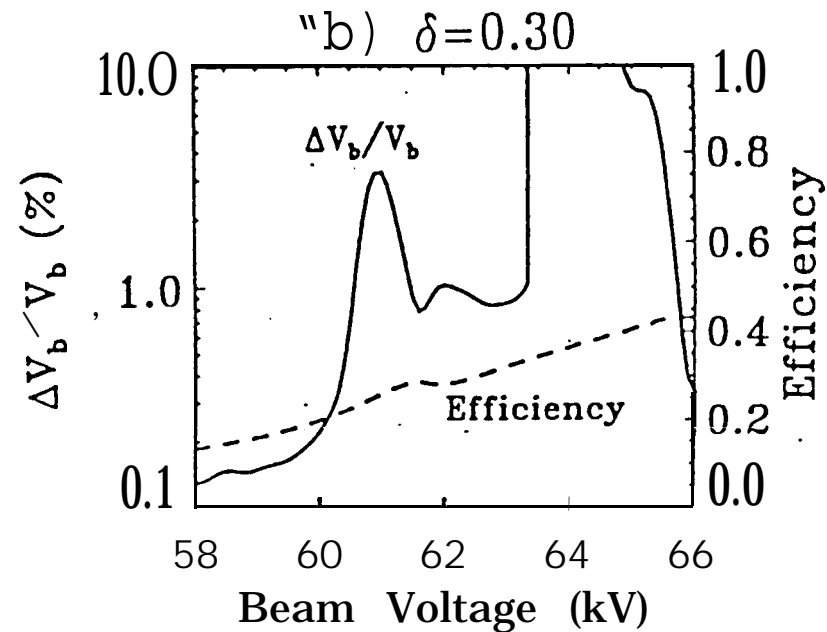
Figure **Allowed Voltage Fluctuation** for Phase Locking

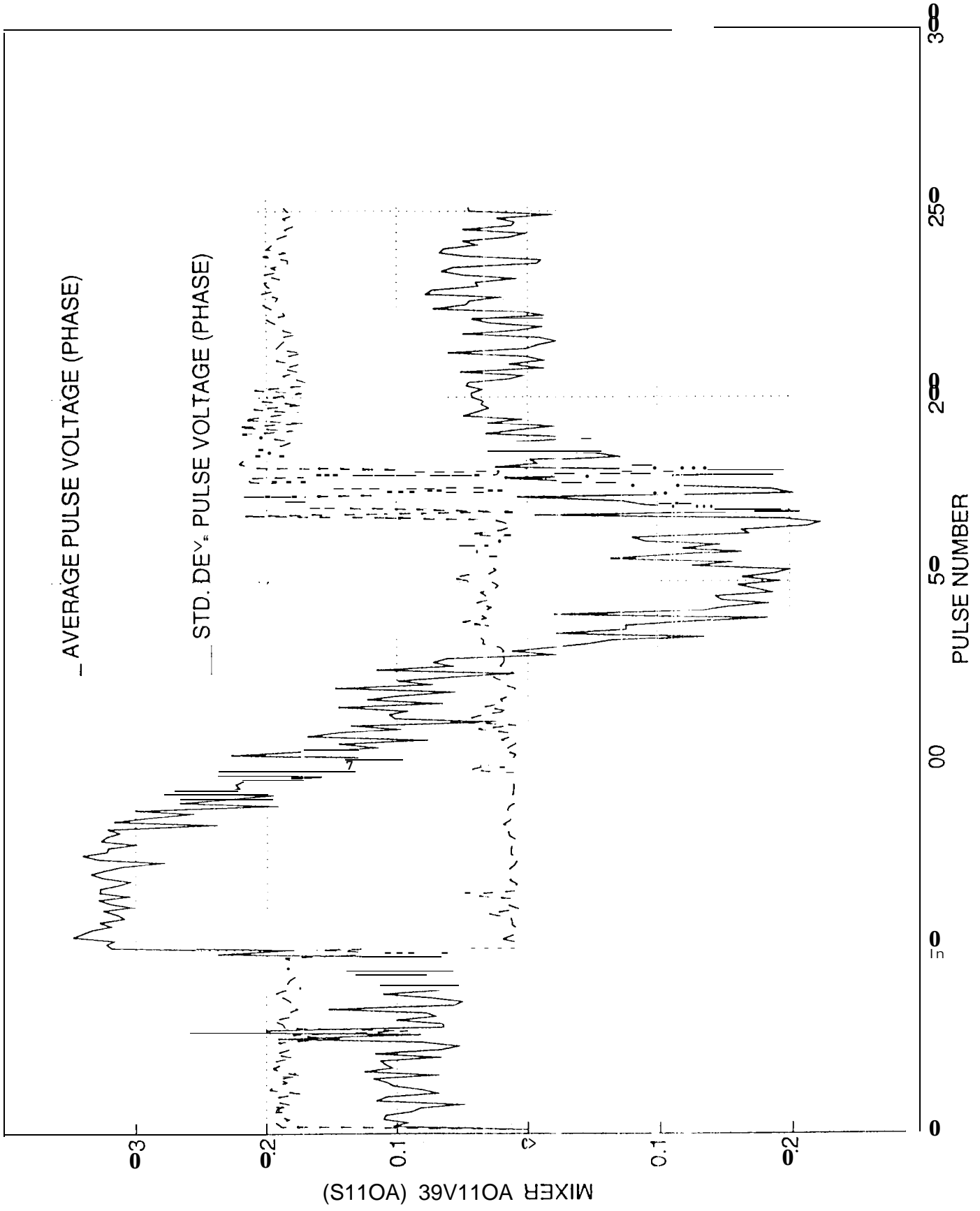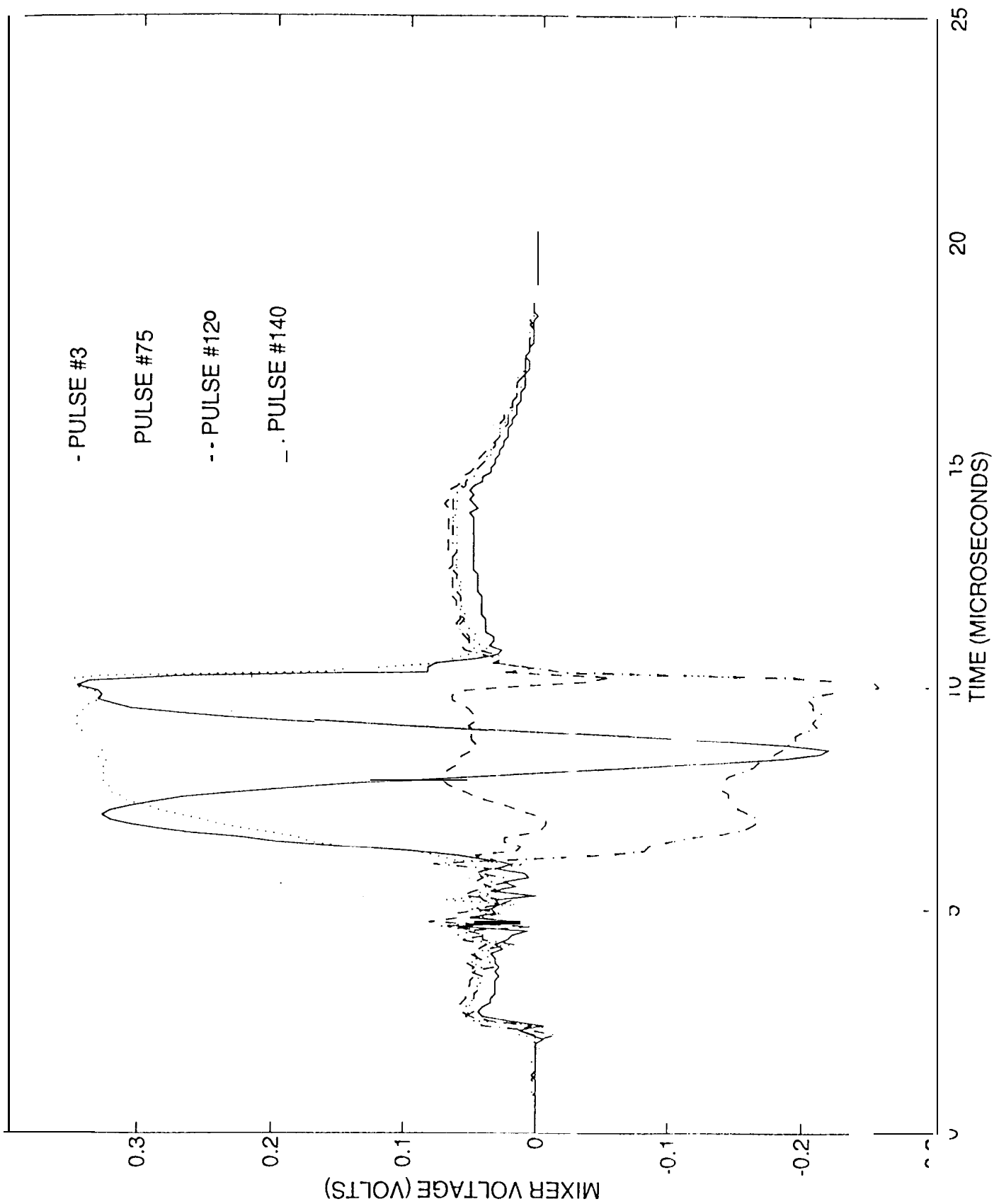AVERAGE PULSE VOLTAGE (PHASE)

STD. DEV. PULSE VOLTAGE (PHASE)

PULSE NUMBER

MIXER VOLTAGE (VOLTS)

AVERAGE PULSE VOLTAGE (PHASE)

STD. DEV. PULSE VOLTAGE (PHASE)

PULSE NUMBER

MIXER VOLTAGE (VOLTS)

FIG 3

FIG. 10